Characterization of a Poly(ethylene oxide)-Poly(propylene oxide) Triblock Copolymer (EO_{27}-PO_{39}-EO_{27}) in Aqueous Solution

Otto Glatter* and Günther Scherf

Institute of Physical Chemistry, University of Graz, A-8010 Graz, Austria

Karin Schillén and Wyn Brown

Department of Physical Chemistry, University of Uppsala, S-75121 Uppsala, Sweden

Received January 25, 1994; Revised Manuscript Received July 19, 1994®

ABSTRACT: We have studied the poly(ethylene oxide)-poly(propylene oxide) triblock copolymer (EO_{27}-PO_{39}-EO_{27}) in aqueous solution in a wide range of temperatures and concentrations. In this paper we present a phase diagram which is based on small-angle X-ray scattering, ultrasonic speed measurements, differential scanning calorimetry, low-shear viscosimetry, and light transmission measurements. We find a broad transition from unimers to micelles with increasing temperatures. The micelles have close to spherical symmetry with a core-shell structure and an outer layer that can be described as a star micelle. The micelles grow in size with temperature, and phase separation with clouding takes place at temperatures above 85 °C. A stiff gel is found at concentrations above 24% (w/w).

I. Introduction

PEO-PPO-PEO triblock copolymers are widely used, nonionic, surface-active agents.[1,2] They are low molecular weight substances known as poloxamers, synperonics, and pluronics; the presently used material EO_{27}-PO_{39}-EO_{37} (designated Synperonic P-85) has a unimeric molecular weight of ~4650, of which about 50% corresponds to the PEO moiety. Such triblock copolymers consisting of a central block of poly(propylene oxide) (PPO) and blocks of poly(ethylene oxide) (PEO) at each side have recently attracted great interest because of their unusual physical properties when dissolved in water.[3-6] It is well-established that PPO is hydrophobic at high temperatures while it is hydrophilic at low temperatures. The amphiphilic character leads to aggregation and surface-active properties which depend on the block lengths.[7] Zhou and Chu[3] studied the aggregation behavior of aqueous solutions of EO_{13}-PO_{30}-EO_{13} (Pluronics L-64, $M_w \sim 2900$) using light scattering. They showed that micelles are formed above a critical copolymer concentration and above a characteristic temperature. They also described an "anomalous" association behavior; this, however, appears to be characteristic of the special preparation and could be eliminated by filtration. No such anomalous behavior was found in their subsequent study on Pluronics F-68.[4] The fact that no sharp CMC is observed was attributed to a possible molecular weight distribution. Further light scattering studies by Wanka, Hoffmann, and Ulbricht on F-127[5] and Brown et al.[6] on P-85 confirmed a transition from dispersed unimers to micelles and, in addition, revealed a very sharp sol-to-gel transition. The micelles and the gel phase in synperonic materials were studied recently by neutron scattering.[8-10] In these studies it was concluded that the interactions in the micellar solutions below the gel phase can be described by a hard sphere interaction model and that a body-centered cubic phase is found at a volume fraction $\phi \geq 0.53$. Upon the application of low shear, the polycrystalline phase abruptly transforms into a single crystal.

In this paper we present detailed studies on the different phases and their temperature dependent transitions based on small-angle X-ray scattering and on complementary techniques: ultrasonic speed measurements, differential scanning calorimetry, low-shear viscosimetry, and light transmission.

The aim of this work was to obtain a more detailed picture of the structure of the micelles and to combine this information on the different gel phases and their boundaries in a phase diagram. Also of special interest were the interactions between the micelles in the higher concentration regime, as can be inferred from the SAXS experiments.

In this paper we present a phase diagram which is based on the different experiments mentioned above. It shows the regimes in concentration and temperature where mostly unimers exist, a broad band of micelle formation, the stiff gel found at high concentrations (≥24% (w/w)) and temperatures around 40 °C, and the existence of a cylindrical micelles/hexagonal phase at even higher temperatures. Phase separation with clouding takes place at very high temperatures (≥85 °C). We find that the micelles have close to spherical symmetry with a core-shell structure and an outer layer that can be described as a star micelle. These micelles become increasingly deformed with increasing concentration which is in contradiction to the simple hard sphere interaction model.[8-10] Also the stiff gel phase shows differences in structure with changing temperature and concentration.

We use small-angle X-ray scattering data to characterize the different phases and more simple complementary techniques to determine the phase boundaries.

II. Experimental Section

A. Sample. The triblock copolymer Synperonic P-85 was obtained from Serva AG, Heidelberg, West Germany. Since P-85 and similar materials are known to contain small contaminating quantities of the diblock copolymer, the sample was purified by Søren Hvidt, Roskilde University, Denmark, using a purification procedure similar to that given in the paper by Reddy et al.[11] The amount of the second peak in the HPLC, attributed to the diblock copolymer in the unpurified sample, constituted a few percent.[6] All previous studies[6-10] were performed using unpurified samples.

B. Small-Angle X-ray Scattering (SAXS). SAXS experiments were performed with a Kratky-Compact-Camera (Anton Paar KG Graz) on a conventional X-ray generator with a sealed tube operated at 50 kV and 50 mA. The camera was modified to allow an easy change from a step-scanning mode to multi-

* To whom correspondence should be sent, including requests for reprints.

® Abstract published in *Advance ACS Abstracts*, September 1, 1994.

0024-9297/94/2227-6046$04.50/0

channel detection using a position-sensitive detector with a metal wire (M. Braun, München, West Germany). A monochromator was not used. The contribution from the copper K_β line[12] was taken into account in the numerical procedures to correct for instrumental broadening.[13-15]

Absolute intensity measurements were not performed in this study. All experiments presented here were performed using the position-sensitive detector in the 4k resolution mode where each channel corresponds to a spacing of 31.7 μm measured at a sample to detector distance of 21.6 cm, leading to a spacing of $\Delta h = 6 \times 10^{-3}$ nm^{-1} in terms of the scattering vector $h = 4\pi/\lambda \sin(\theta/2)$, where λ is the wavelength of the Cu Kα line (0.154 nm) and θ is the scattering angle. The size of the primary beam at the sample position was about 1.5 × 0.015 cm; the scattering curves were recorded in 950 channels during a time of 15 000 s with a typical count rate of 2–20 counts/s depending on the channel number, concentration, and temperature.

Each scattering curve was measured at least four times. After averaging and subtraction of the averaged water file, the smeared data were corrected for instrumental broadening. The result of these calculations is a smooth approximation curve to the smeared data, a desmeared scattering function, and in the case of dilute systems, the distance distribution function $p(r)$ of the particle which is the Fourier transform of the scattering function and which can be used for further interpretation.[16,17]

$$I(h) = 4\pi \int_0^\infty p(r)[(\sin hr)/hr]\, dr \qquad (1)$$

The convolution square root technique is used to deconvolute the $p(r)$ function of micelles into the radial density profile $\rho(r)$ assuming spherical shape[18-20]

$$p(r) = r^2\langle \tilde{\rho}^2(\mathbf{r})\rangle = \langle \int \rho(\mathbf{x})\, \rho(\mathbf{x}-\mathbf{r})\, d\mathbf{x}\rangle \qquad (2)$$

where $\langle\ \rangle$ stands for the spherical average and $\tilde{}^2$ is a symbol for the convolution square operation.

C. Ultrasonic Speed Measurements (USM). The speed of sound waves is a function of the adiabatic compressibility and the density of the fluid.[21] The compressibility of solutions is a function of the temperature and of the solute properties. The speed of sound can be measured with high precision in a pulsed mode experiment, where the time required for a short pulse to travel through a well-defined sample cell (total filling volume <2 mL) is used to calculated the speed with an accuracy of ±1 m/s (DSA 48, Anton Paar KG, Graz, Austria). No frequency dependence is measured with this instrument.

The technique will be briefly described below and a more detailed description of this measuring technique and of the low-shear viscosimetry (following section) will be given elsewhere.[22] At low concentrations the speed of sound depends linearly on the amount of solute in the solution. Structural changes within the solute molecule may also change the speed of the sound wave. In addition, there is a further dependence on the number of particles in the solution at fixed concentration. It is thus possible, for example, to follow the hydrolysis of sucrose into glucose and fructose.

Since micelle formation reduces the number of particles, we therefore expect a reduction in the speed of sound. These changes are small, so the "specific speed" (S_s) of the pulses is used:

$$S_s = \frac{S_{\text{solution}} - S_{H_2O}}{S_{H_2O}} \qquad (3)$$

The specific speed is the change of the speed in the solution (S_{solution}) relative to the speed in water (S_{H_2O}). The changes can be best visualized by taking the *negative first derivative of the specific speed* S' with respect to the temperature T:

$$S' = -\frac{d(S_s)}{dT} \qquad (4)$$

In a plot of S' versus temperature (T), the formation of micelles will result in a peak which develops from a flat background. In order to compare data at different concentrations, we divide the data by the concentration.

USM has already been used by Rassing and Attwood[23] to follow the formation of micelles, but they used a different measuring technique and followed another line of data treatment.

D. Low-Shear Viscosimetry (LSV). The mechanical oscillator method is widely used in precision densimetry.[24,25] This method is based on the measurement of the eigenfrequency of a U-shaped glass tube filled with the sample. This frequency is slightly changed by damping forces in viscous samples. The ratio of the damping force to the elastic forces of the glass must be determined to correct for such effects and to determine the density of the fluid.

We use here a modified version of the standard setup (DMA 58, A. Paar KG, Graz, Austria) which allows the direct measurement of this damping ratio operating in the first-order mode of oscillation. A more detailed description of the technique is given elsewhere.[22] The essential point is that the measured damping ratio DR is related to the viscosity η of the fluid.

There is a linear dependence of DR on $\sqrt{\eta}$ for small viscosities. This function runs through a maximum at $\eta^* \sim 600$ mPa s and goes to zero at high values of η, where the fluid is no longer streaming in the tube but acts like a stiff rod.

In order to be able to understand the resulting diagrams it is important to recognize that all data shown in the figures correspond to the difference between the DR values for the solution and the solvent, in the present case water. This means that at high η values, where one expects negligible damping ($\eta \gg \eta^*$) we see negative values which correspond to the damping of water.

The method is thus not suited to "measure" viscosity quantitatively over a wide range of concentrations, but it has the advantage that the fluid is in a closed, well-thermostated glass tube and that the shear strain is negligible. The volume of the tube is about 1 mL. It should be mentioned, however, that it is not possible to vary the frequency (the tube oscillates at the eigenfrequency) and that it is not possible to measure the elastic and loss moduli G' and G'' of the sample.

E. Differential Scanning Calorimetry (DSC). This technique has been used as an independent control experiment to USM and to the low-shear viscosimetry experiments. We used a Perkin-Elmer DSC 4 with a scan rate of 5 K min^{-1}.

F. Light Transmission (LT). Light transmission measurements can be used to detect phase separation. When a system demixes into two nonmiscible phases, the system becomes turbid due to multiple scattering and this reduces the transmittance of light even if the two phases do not absorb light.

The transmittance of light was measured in a light scattering goniometer equipped with a temperature-controlled sample holder for cylindrical cuvettes with a diameter of 10 mm. The light source was an argon-ion laser (Spectra Physics, 2020 Series, 1 W, 514 nm). The intensity of the transmitted light was measured with a photodiode operated in the linear regime. This gives directly the current of the photodiode as a measure of the transmitted light intensity.

III. Results

A. SAXS. SAXS was used to obtain information on the size and structure of the unimers and the micelles as well as on the interaction between the micelles with increasing concentration. SAXS can also be used to study the structure of the stiff gel at concentrations above 24% (w/w).

1. Formation of Micelles (5% (w/w)). In the first data series the results are shown for a 5% (w/w) solution of P-85 in water at temperatures between 10 and 70 °C. Our experimental setup did not allow measurements above 70°. The overall contrast (difference in electron density) of the sample in water is very low. The electron density of water at 20 °C can be estimated to be 334 e nm^{-3}, the difference in water for PEO blocks is +49 e nm^{-3} and for PPO blocks it is +25 e nm^{-3}.[30] So it was necessary to measure this series at the rather high concentration of 5%

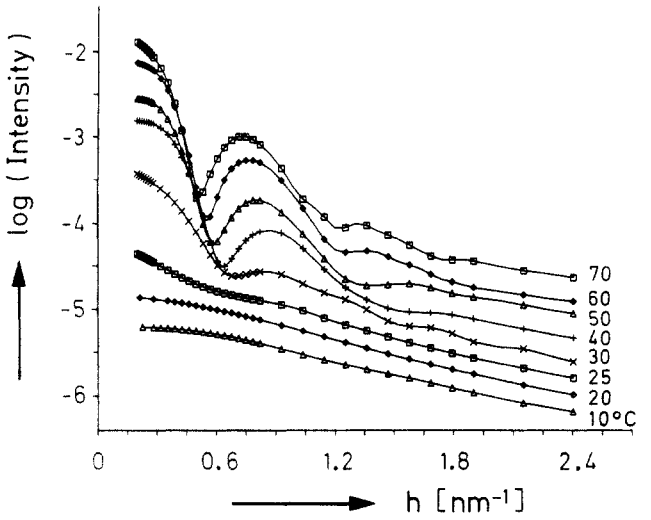

Figure 1. Temperature dependence of the desmeared scattering functions of 5% (w/w) P-85 (curves shifted by a constant factor).

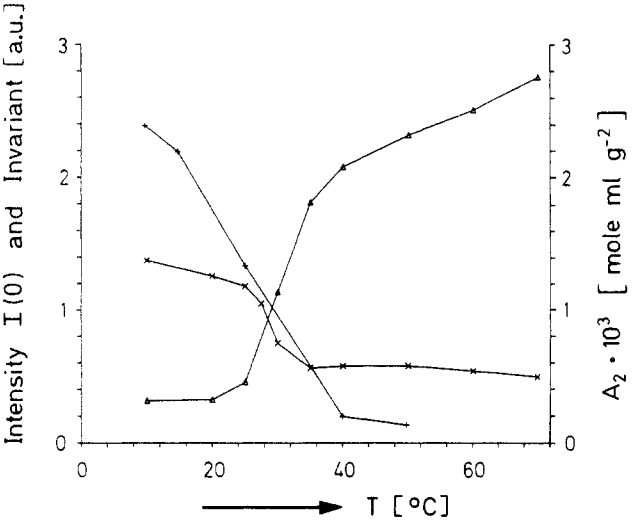

Figure 2. Temperature dependence of the scattering intensity at zero angle (△) and of the *invariant* of a 5% (w/w) P-85 solution (×). The values of the second virial coefficient A_2 from light scattering experiments[6] are included in this plot for comparison (+).

(w/w) to obtain reasonable counting statistics. Figure 1 shows the desmeared scattering curves (corrected for instrumental broadening and K_β radiation) after averaging and subtraction of the background.

At low temperatures (10–20 °C) the flat scattering curves of the unimers are observed. The radius of gyration is R_g = 1.4 nm. The overall structure of the chain cannot be determined from such data. It is possible to fit the data points with the Debye function for a Gaussian chain as mentioned in ref 10, but many other structures are possible.

At temperatures above 20 °C an increase in intensity at low h values is observed with the formation of a side maximum typical for spherical micelles. This structure is already well-developed at 40 °C. It is seen from this figure that the scattering curves are similar for temperatures between 40 and 70 °C and, in addition, the position of the minimum and the first side maximum is shifted to smaller h values corresponding to a growth of the micelles. In order to determine the particle size and internal structure it is necessary to measure at lower concentrations (see below).

Although the forward scattering intensity (at zero angle) is influenced by interparticle scattering contributions, it is relevant to look at its temperature dependence. This is given in Figure 2 together with the invariant and the second virial coefficient A_2 from light scattering data.[6]

There is a constant intensity up to about 20 °C, followed by a strong increase during micelle formation up to about 40 °C and thereafter a nearly linear increase during the growth of the micelles up to 70 °C.

The formation of micelles results since water is a nonsolvent for PPO above 14 °C. This leads to a decrease in the second virial coefficient, as demonstrated earlier using static light scattering.[6] These A_2 values are included in Figure 3 for comparison.

A similar effect is seen in the SAXS data at a single concentration (5% (w/w)). The second moment of the scattering function is termed the *invariant* since it does not change if the particle shape changes without alteration in the internal structure.[14] It is important to note that the invariant is proportional to the mean square fluctuation of the electron density ($\Delta\rho^2$). The invariant is no longer constant if the latter quantity varies, as is the case during the formation of micelles. The PPO chains can dissolve in water at lower temperatures but form the hydrophobic core of the micelles at higher temperatures. During this process the mean square fluctuation of the sample is reduced and the invariant decreases as shown in Figure 2.

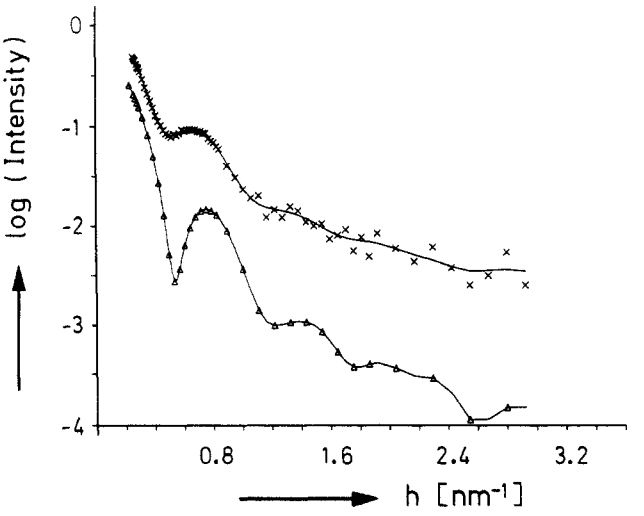

Figure 3. Scattering functions of a 1% (w/w) P-85 solution at 50 °C: (×) smeared scattering function after subtraction of water data; (—) best fit to this curve by the desmearing routine; (△) desmeared scattering function.

2. Structure of the Micelles (1% (w/w)). It was mentioned above that the overall contrast for X-rays of P-85 in water is low and that interparticle scattering is not negligible at 5% (w/w), which is a concentration giving reasonable counting rates. In order to study the structure of the micelles it is necessary to reduce the concentration to 1% (w/w) at 50 °C, where the contrast is still sufficiently good for the extraction of structural information and where interparticle scattering contributions can be neglected. The results in reciprocal space are shown in Figure 3.

The influence of instrumental broadening can be seen on comparing the smeared and desmeared data. The corresponding $p(r)$ function is shown in Figure 4. The interparticle contributions, which lead to oscillations in the range of high r values at 5% (w/w) (results not shown), are negligible at a concentration of 1% (w/w).

It is possible to directly calculate the radial electron density distribution $\rho(r)$ from the distance distribution function $p(r)$ by assuming spherical symmetry.[18-20] This

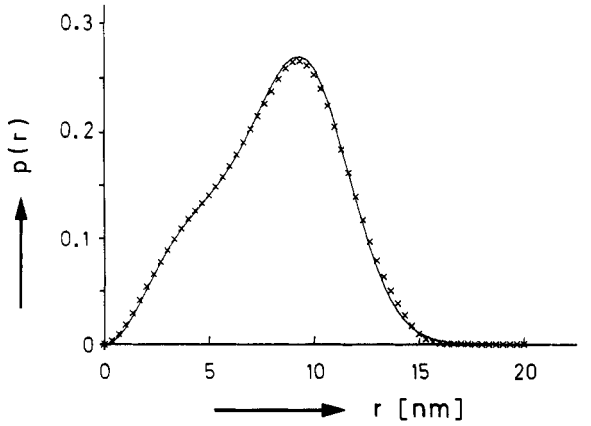

Figure 4. Distance distribution function of 1% (w/w) P-85 (×) together with the corresponding function of the best-fitting spherically symmetric particle (full line).

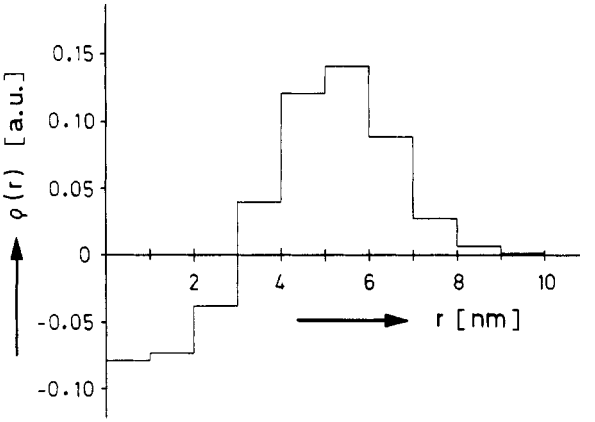

Figure 5. Radial electron density difference compared to water in arbitrary units for 1% (w/w) P-85 micelles.

procedure would fail, if this assumption is not fulfilled. In this case the procedure would not allow fitting of the $p(r)$ function with reasonable accuracy. It should be mentioned that for mathematical reasons $\rho(r)$ is expressed in this technique by a series of step functions. Any smooth curve having the same area would give the same fit to the data since the resolution of these experiments is rather low.

The result of such a deconvolution is given in Figure 5. The abscissa represents the level of the electron density of water. The hydrophobic PPO core has a slightly lower density and a radius of about 2.5–3 nm, while the PEO shell has a density which is higher than water and shows a decreasing density with an outer radius of about 8 nm. This density profile is in good agreement with a picture of a star-shaped micelle, consisting of a compact PPO core and a soft PEO shell with starlike arms extending into the water phase. The electron density of the shell decreases monotonically in such a model.[26] After calculating the electron density profile of the best fitting spherically symmetric object, one can compute the corresponding $p(r)$ function, and this is shown as the full line together with the original data in Figure 4. The negative electron density in the core is in disagreement with the excss density of 25 e nm^{-3} for the PPO block in water at 20 °C. Current precision density measurements show a distinct decrease of the P-85 solution density during formation of micelles (unpublished results). This reduction can be explained by an increase of the specific volume for the PPO block[30] leading to a reduction of the electron density in the core.

3. Interactions between Micelles. Intermicellar interactions can also be studied using SAXS. The scattering functions of P-85 solutions at 40 °C and at

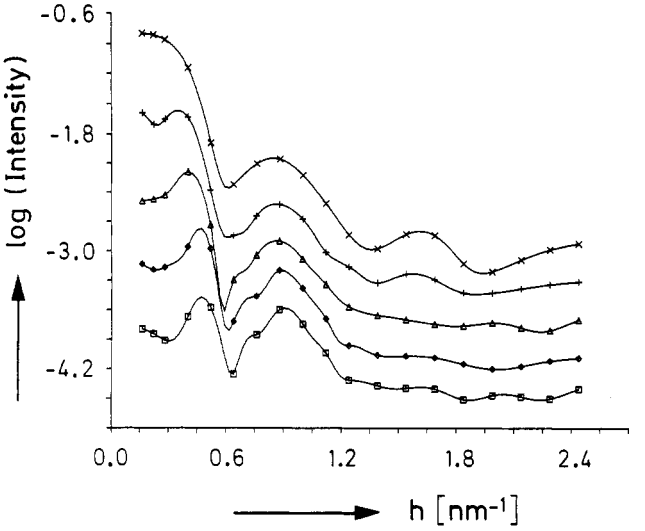

Figure 6. Scattering curves of P-85 solutions at 40 °C at different concentrations: (x) 5% (w/w); (+) 10% (w/w); (△) 15% (w/w); (◇) 20% (w/w); (□) 25% (w/w).

concentrations between 5% (w/w) and 25% (w/w) were measured. All data were treated in the same way to minimize artefacts. After subtraction of the water file, the data were desmeared using the indirect transformation technique in reciprocal space.[14] The resulting desmeared scattering curves are shown in Figure 6.

For spherical particles, the total scattering intensity $I(h)$ can be written as the product of the particle form factor $P(h)$ times the structure factor $S(h)$ describing the influence of interparticle scattering. The function $S(h)$ is a constant for infinite dilution and shows a pronounced maximum with damped oscillations toward higher h values with increasing concentration. The position of the first maximum is related to the interparticle distance. Figure 6 shows that such a maximum can be found already at 10% (w/w) and it increases in height and is shifted to higher h-values with increasing concentration. The shift in the position corresponds to a decrease in the mean distance between the micelles with increasing concentration. For concentrations of 15% (w/w) and greater a second maximum is introduced by the structure factor at $h \sim 0.7$ nm^{-1}.

The overall size of the micelle is the same for all concentrations at constant temperature. This is deduced from the unchanged position of the first minimum and of the first side maximum of the form factor (compare with Figure 1, where the minima and maxima are shifted to smaller h values on micellar growth). Another important finding is the fact that the second side maximum of the form factor of the micelles disappears at higher concentrations. This fact can be explained by an increasing perturbation of the spherically symmetric structure of the soft outer PEO shell of the micelle. A third important fact is the observation that the two curves for 20% (w/w) and 25% (w/w) are nearly identical and do not show evidence for any essential structural differences in the solutions. This is important since there is a dramatic change in the viscosity of the sample in this concentration regime. The solution is a fluid with rather low viscosity up to 23% (w/w) and a stiff gel at concentrations higher or equal to 24% (w/w) (see the following sections). This means that the micelles interact strongly with possible entanglements between PEO chains, without essentially changing the mutual arrangement in the structure.

A similar picture emerges on crossing the area corresponding to the stiff gel on increasing the temperature

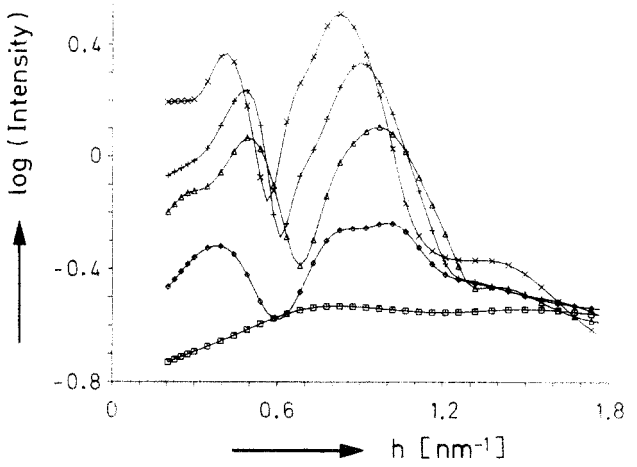

Figure 7. Scattering curves of a 25% (w/w) solution of P-85 at different temperatures: (□) 10 °C; (◇) 20 °C; (△) 30 °C; (+) 40 °C; (×) 55 °C.

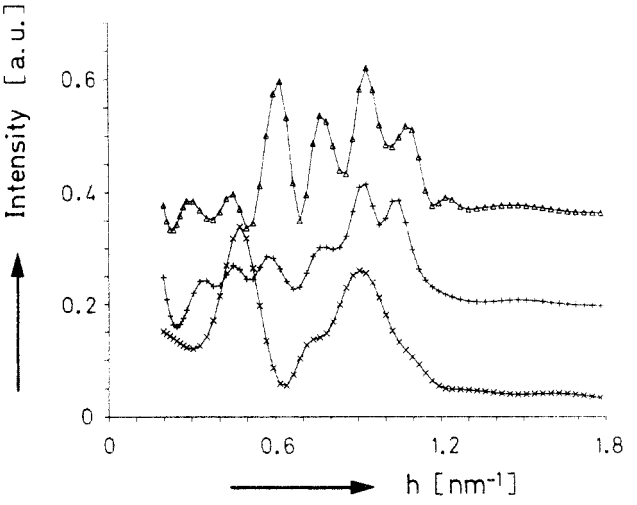

Figure 8. Scattering curves of P-85 solutions at 40 °C and concentrations of 25% (w/w) (×), 30% (w/w) (+), and 35% (w/w) (△).

at the fixed concentration of 25% (w/w) (Figure 7). The desmeared scattering curves at five different temperatures are shown in this figure. At 10 °C there is a dense solution of mostly unimers (micelle formation starts above 8 °C). At 30 °C there is a solution of micelles containing some unimers. The stiff gel exists between 32 and 48 °C. The two curves at 30 and 55 °C thus represent micellar solutions of low viscosity while the data at 40 °C correspond to the stiff gel. There is a continuous development to larger micelles but otherwise no significant changes are observed when entering the gel phase.

The stiff gel is not a single phase throughout its range of definition. This can be seen from the scattering data at 40 °C at different concentrations (25–35% (w/w)). The desmeared scattering data are shown in Figure 8. The data for the 25% solution still show the features of a concentrated solution of micelles (similar to the data from 20%). However, the picture changes essentially for 30 and 35% (w/w). That the interaction peak at around 0.4 nm^{-1} disappears and is replaced by a series of approximately equidistant peaks is apparent especially in the 35% (w/w) data. These oscillations cannot be smoothed out without introducing systematic deviations between the approximation curve and the data points. Such a periodic oscillation could be explained by a lamellar structure. The spacing of these peaks is 0.155 nm^{-1}, giving a repeat distance of $2\pi/0.155 = 40.5$ nm (the first-order peak is missing due to limited resolution). Another possibility of interpretation could be the coexistence of two different structures. Further investigations will be needed to clarify the structure of the stiff gel over its whole range of existence.

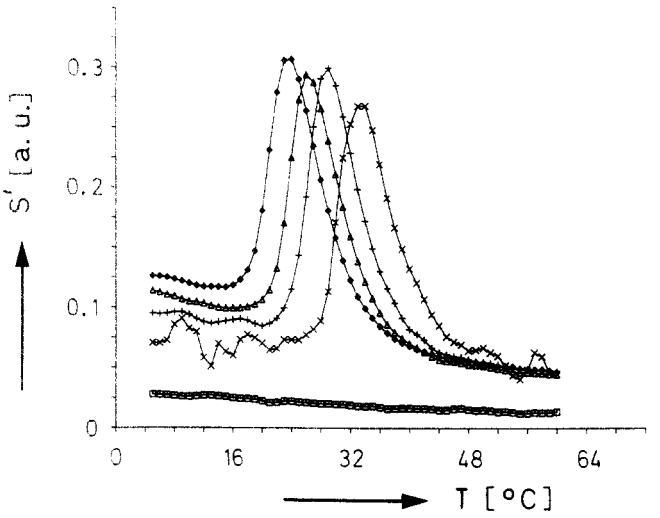

Figure 9. Temperature dependence of USM data for different concentrations of P-85: 1% (w/w) (x); 5% (w/w) (+); 10% (w/w) (△); 15% (w/w) (◇); 10% (w/w) sucrose solution (□).

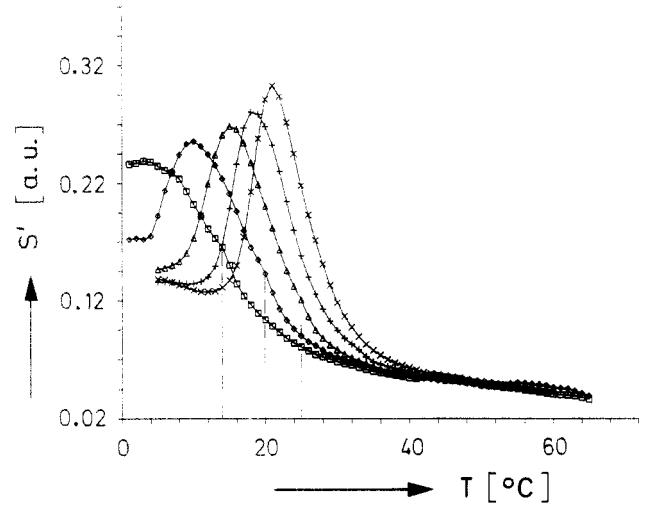

Figure 10. Temperature dependence of USM data for different concentrations: 20% (w/w) (×); 25% (w/w) (+); 30% (w/w) (△); 35% (w/w) (◇); 40% (w/w) (□).

B. USM. These measurements allow the determination of the temperature range where the unimers aggregate into micelles. Figure 9 shows the temperature dependence of P-85 solutions together with data for a 10% (w/w) sucrose solution as a reference. The signals have been divided by the corresponding concentration.

The sucrose solution shows monotonically decreasing behavior. The curve for 5% (w/w) P-85 is similar only at low and high temperatures. Deviations from the temperature dependence of sucrose start at about 20 °C (micelles start to form), show a clear maximum at 29 °C (corresponding to the highest micelle formation rate), and vanish at about 45 °C. This signal develops in good agreement with the SAXS data (Figure 1), but the experiments are much faster and more easily made. A similar behavior is found for all other concentrations.

Figure 10 shows USM data for the concentration regime ranging from 20% (w/w) up to 40% (w/w) (all data divided by the concentration). The effect is linear up to about 20%, and the peak shifts to lower temperatures with

Table 1. Phase-Boundary Temperatures (°C)[a]

conc of	USM				DSC		LSV		LT		
P85 (wt %)	T_L	T_M	T_U	T_α	T_M	T_α	T_α	T_ω	T_A	T_B	T_C1
1	21	33.5	56								87
5	17	29	49		30						88
10	13	26	45								89
15	11	23.5	42								91
20	10	21	39		22						96
24							36	39			
25	8	18.5	37		19		32	48			94.5
27.5					17	27.5	28	58			94.5
30	4	15	34	25	14	24	25	60	61	67	94
35		10	31	20	13	20	20		55	61	93
40		4	28	14	(8)	15	15		43	51	91
σ	±2	±0.5	±3	±1	±1	±1	±1	±1	±1	±1	±0.5

[a] Micelle formation: begin (T_L), maximum formation rate (T_M), end (T_U). Stiff gel: lower boundary (T_α), upper boundary (T_ω). Clouding limits: T_A, T_B, T_C (transmittance ≤0.05).

increasing concentration. These curves allow the estimation of the transition regime from unimers to micelles, as defined by the temperatures for the onset of the peak, the peak maximum, and the point at which the peak disappears. Numerical values for these temperatures T_L, T_M, and T_U are given in Table 1.

It should be noted that a little side hump is visible at the highest concentrations (30–40%) marked with dashed lines. This position agrees with the transition into the stiff gel, but it is impossible to determine the transition temperature precisely from the USM data.

C. LSV. It was already discussed in the previous sections that P-85 solutions may be liquidlike with low viscosity. Soft and stiff gels can also form at higher temperatures and/or concentrations. In the following two figures (Figures 11 and 12) the temperature dependence of the damping ratio is shown for different concentrations. It should be recalled at this point that the damping ratio is related to the viscosity η.

At 5% (w/w) one observes the typical decrease of the viscosity with temperature up to about 30 °C, followed by a slight increase due to the formation of the micelles up to about 65 °C. Above this temperature a soft gel is formed. Our SAXS experiments were limited by the temperature control unit to $T \leq 70$ °C. The viscosity increases with concentration, but the temperature dependence is similar up to about 15% (w/w).

At concentrations of 20% (w/w) and above, pregelation with a maximum between 30 and 40 °C is observed. This situation changes dramatically at concentrations above 23% (w/w), as can be seen in Figure 11b. At 24% (w/w) the stiff gel is observed at temperatures between 36 and 39 °C (see also Table 1). The damping ratio becomes zero for very high viscosities, as already discussed in section II.D. After the subtraction of the damping values for water, negative values are obtained. This stiff gel region becomes wider with increasing concentration. After the "melting" of the stiff gel, it is succeeded by formation of a soft gel at temperatures above 65 °C.

The high-temperature behavior (formation of the soft gel) starts to change at 27.5% (w/w) (Figure 12). In this regime phase separation (clouding) is observed.

D. DSC. It is well-known that the formation of micelles can also be seen in DSC experiments as an endothermic peak in the heating cycle.[5,6] The present DSC results (Figure 13) provide excellent confirmation of the USM and LSV results.

The maximum shifts to lower temperatures with increasing concentration (compare with Figures 9 and 10!). A small additional peak is observed at temperatures between 15 and 35 °C for the higher concentrations at which the stiff gel is formed. The corresponding temperatures are in excellent agreement with the LSV data

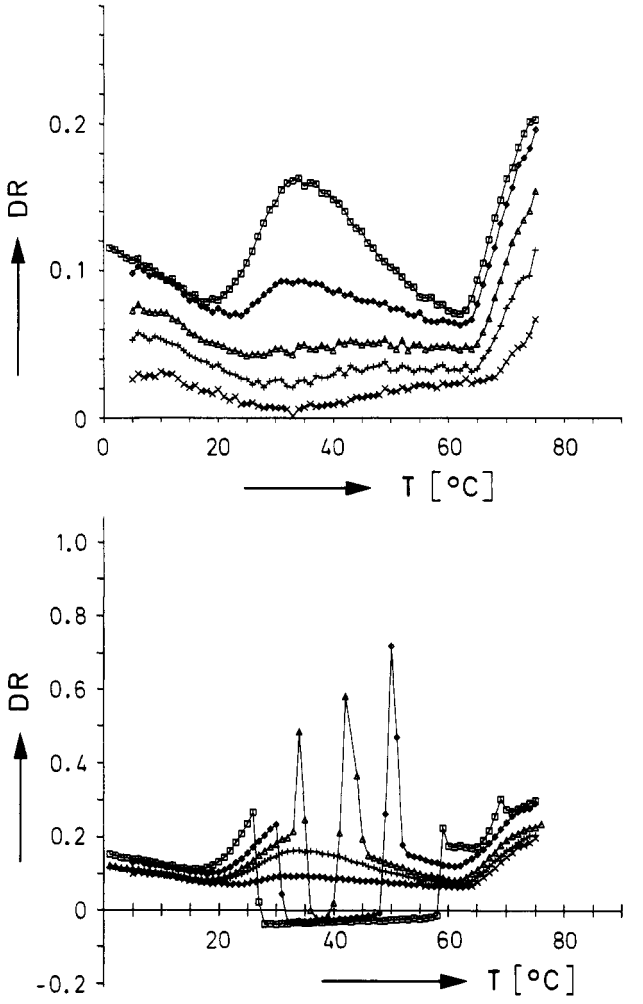

Figure 11. (a, upper half) Damping ratio of the first-order mode oscillation of P-85 solutions after subtraction of water data: 5% (w/w) (×); 10% (w/w) (+); 15% (w/w) (△); 20% (w/w) (◇); 23% (w/w) (□). (b, lower half) Damping ratio of the first-order mode oscillation of P-85 solutions after subtraction of water data: 20% (w/w) (×); 23% (w/w) (+); 24% (w/w) (△); 25% (w/w) (◇); 27.5% (w/w) (□). Negative values indicate very high viscosity (stiff gel).

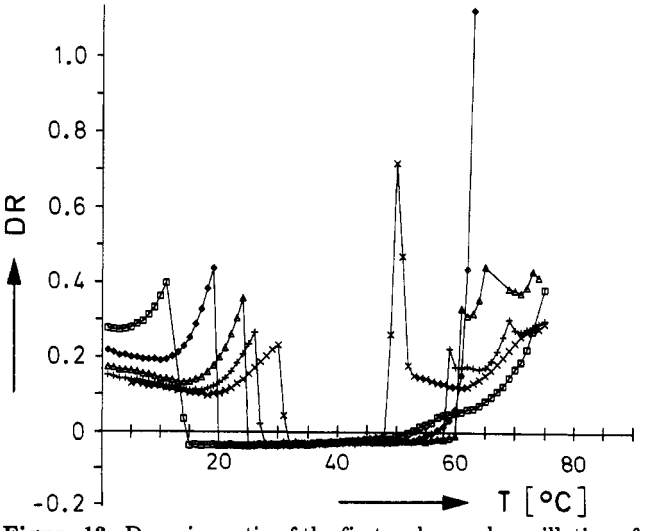

Figure 12. Damping ratio of the first-order mode oscillation of P-85 solution after subtraction of water data: 25% (w/w) (×); 27.5% (w/w) (+); 30% (w/w); (△); 35% (w/w) (◇); 40% (w/w) (□). Negative values indicate very high viscosity (stiff gel).

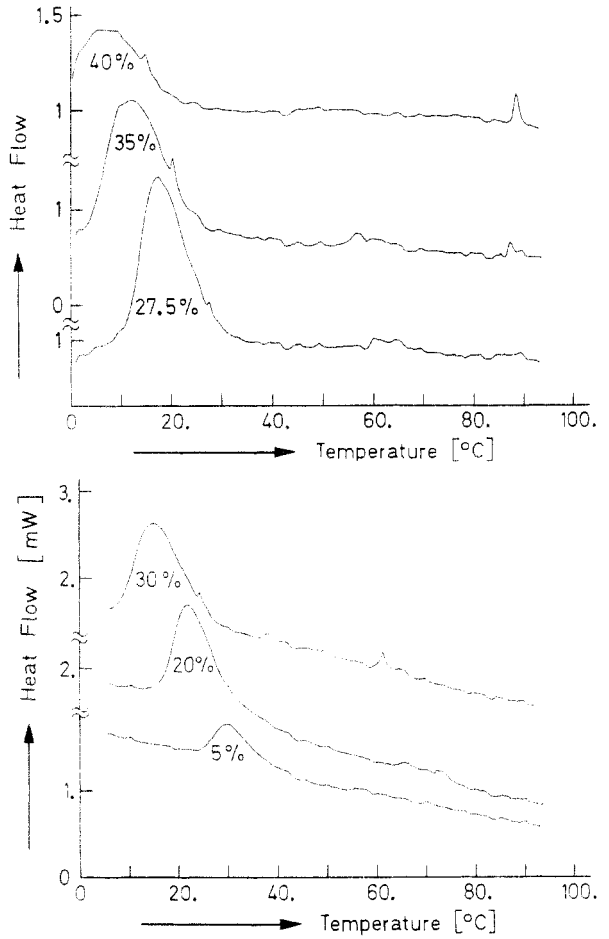

Figure 13. (a, upper half) DSC scans for P-85 solutions at 5% (w/w), 20% (w/w), and 30% (w/w). (b, lower half) DSC scans for P-85 solutions at 27.5% (w/w), 35% (w/w), and 40% (w/w).

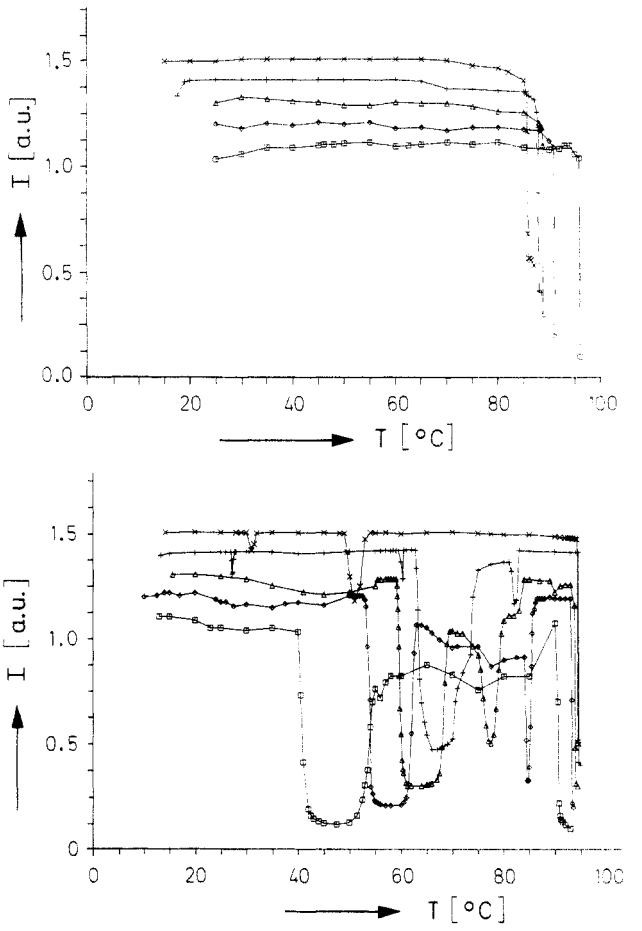

Figure 14. (a, upper half) Transmitted intensity of P-85 solutions, measured by a photodiode, as a function of temperature: 1% (w/w) (□); 5% (w/w) (◇); 10% (w/w) (△); 15% (w/w) (+); 20% (w/w) (×). Curves are vertically shifted by a constant. (b, lower half) Light transmission of P-85 solutions as a function of temperature: 25% (w/w) (×); 27.5% (w/w) (+); 30% (w/w) (△); 35% (w/w) (◇); 40% (w/w) (□).

(see Table 1). These peaks were found in all experiments, while the small amplitude peaks at $T \geq 60$ °C were not reproducible.

E. LT. Light transmission experiments were performed to determine the two-phase regions. Phase separation leads to clouding due to multiple scattering and to a reduction of the transmittance.

Results for concentrations up to 20% (w/w) are shown in Figure 14a. The normalized photodiode current providing a direct measure of the transmitted light intensity has been shifted by multiplication with a constant factor for clarity. The cloud point increases from 87 °C for 1% (w/w) to 96 °C for 20% (see Table 1). There is no change in the light transmission below the cloud point for concentrations below 25% (w/w).

The light transmission diagram at higher concentrations (25–40% (w/w)) is somewhat more complicated, as there is not only clouding at higher temperatures ($T \geq 85$ °C) but also clouding in the regime above the stiff gel (see Figure 14b). The transmission decreases to a value below 0.05 in this regime (temperatures T_A and T_B in Table 1). Strong variations of the transmittance above this regime indicate changes in the structure which have not yet been investigated. There is also a measurable reduction of the transmittance close to the boundaries of the "stiff gel" at the two concentrations 25 and 27.5% (w/w).

IV. Discussion

The results from the various techniques can be combined to construct a phase diagram for P-85 solutions in the regime of 0–100 °C and for concentrations up to 40% (w/w). A main feature of this graphical representation (Figure 15) is the broad transition from unimers to micelles. Three lines are used to characterize this transition. Two thin lines describe the start and end of micelle formation, while the dashed-dotted line shows the maximum in the formation rate. These lines were determined from USM data and checked by DSC for some concentrations. The transition regime is marked by vertical hatching. In this regime unimers and micelles coexist. The lower left corner (hatching to the right) below the transition band is the regime consisting mostly of unimers (in coexistence with a small number of large aggregates.[6]

The formation of micelles can only be proved by SAXS experiments. By comparison of these data (for instance at 5% (w/w)) with the USM results, it is seen that this much simpler complementary technique allows us to follow the transition in steps of 1 deg. It is important to mention that the determination of the transition band from SAXS data at higher concentrations would be very difficult if not impossible. Structural details of the micelles can be determined only at concentrations of about 1% (w/w). The SAXS results show that the micelles can be described by a spherical star-shaped structure with a compact core of PPO and PEO arms in the water phase. There is good agreement between the picture of a star-shaped micelle and the radial electron density distribution found from SAXS experiments.

At concentrations below 24% (w/w) we find, above the transition range, a phase with micelles which grow up to

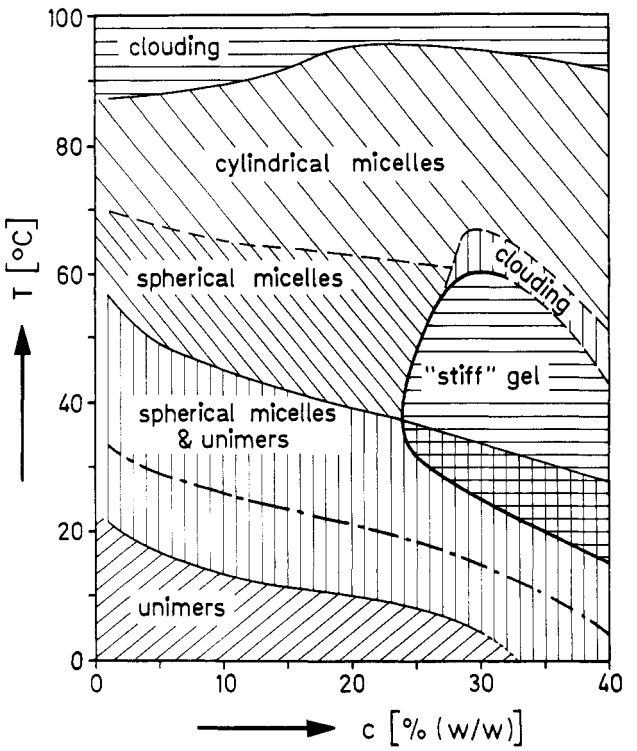

Figure 15. Phase diagram for aqueous P-85 solutions.

a temperature of about 70 °C (hatching to the left). The increase in size is also deduced from the SAXS data as well as from dynamic light scattering results. We were not able to determine the structure existing at temperatures above 70 °C owing to experimental limitations. However, recent dynamic LS results[28,29] clearly show the presence of cylindrical micelles ($L/d \simeq 7$) at low concentrations ($C < 1\%$) in the temperature range 70–85 °C. Above 85 °C the rods become labile and shorter prior to clouding.

The interactions between micelles were studied using a concentration series at a constant temperature of 40 °C. The X-ray data showed that the micelle size is, to a first approximation, unchanged by interactions at higher concentration but that the form factor of the micelles is altered to a scattering curve of a nonspherical particle. The scattering curves are structureless at higher h values, a fact which can be explained by a deviation from spherical symmetry. This can easily be understood with the model of two star-shaped micelle at small distances with interpenetrating PEO shells.

Mortensen and Pedersen[10] made low-resolution neutron small-angle scattering experiments and fitted the data to a hard sphere model of interaction. This is the simplest possible model, allowing a simplified interpretation of the data. These authors do not claim, however, that this is a unique solution. The present data were measured to higher resolution, and the contrast for X-rays is different from that for neutrons. The SAXS results are not in agreement with a hard sphere interaction model since the form factor of the micelles changes with concentration; i.e., the separation into the product of the form factor and the structure factor is no longer valid.

The micellar phase shows increasing viscosity above 65 °C (see the LSV data). This transition is marked by the slightly falling dashed line in Figure 15, where the transition temperatures are obtained from LSV data. We have as yet no data on the structure of this phase, but recent experiments[28,29] show the presence of cylindrical structures. Finally, the system phase-separates at very high temperatures (above 85 °C) with clouding and a dramatic decrease in the light transmission (horizontal hatching in Figure 15).

The region of the stiff gel will now be discussed. This phase is defined by a high viscosity, and the LSV data are used to establish the phase boundaries; this phase is shown by horizontal hatching. The results from LSV are in excellent agreement with the corresponding temperatures determined using DSC, USM, and LT. This is important since the latter three techniques do not apply any shear strain to the sample. The results are thus unbiased by shear thinning. It should be noted that there is a slight disagreement with rheological data obtained using conventional cone–plate oscillatory shear instruments.[27] With improved temperature control in the rheometer, it was possible to reduce these differences to some extent. Remaining differences may be due to shear thinning effects. An interesting detail is the finding that the micelle formation band overlaps with the stiff gel phase; however it should be noted that there is still a fraction of 60% to 76% (w/w) of water in the system in this region.

Above the stiff gel (extending toward higher temperatures) there is a narrow clouded two-phase region at concentrations above 25% (w/w) (vertical hatching in Figure 15).

Structural investigations in the gel phase and above will be continued. Our SAXS data provide no evidence for a micellar cubic crystal, as concluded in ref 10. Changes are observed in the structure at concentrations between 25% (w/w) (similar to those for the micellar solution at 20% (w/w)) and 35% (w/w)—which suggest at least partial contributions from a lamellar structure. Shear forces were not applied to the samples prior to the scattering experiments. Shear-induced crystallization to bcc liquid crystals has been reported recently.[9]

The structure of the stiff gel and that of the phase containing cylindrical micelles require further investigation, although their ranges of existence are now known. There is some evidence from the LSV data that the structure of the latter phase changes on increasing the concentration above 25% (w/w). A hexagonal arrangement of rodlike micelles has been proposed for this region.[9,10,29]

The phase diagram shown in Figure 15 is still incomplete, although clarified to a large extent. A combination of several complementary techniques was necessary to establish the boundaries and areas shown in this phase diagram. Scattering techniques provide much detail regarding the internal structures but they require corroborative data from other independent techniques to yield an unambiguous interpretation.

Acknowledgment. We thank Søren Hvidt (Roskilde University Center) for the purification of the sample and for sending us preliminary results from his rheological experiments. Karl Gruber (University of Graz) is thanked for performing preliminary SAXS experiments and for fruitful discussions. Financial support from the Swedish Natural Science Research Council (NFR), the Swedish Institute, and the Office of International Relations, University of Graz, in support of a 4 month research visit of Karin Schillén to Graz University is gratefully acknowledged.

References and Notes

(1) *Non-ionic surfactants, Physical Chemistry*; Schick, M. J., Ed.; Marcel Dekker: New York, 1987.
(2) Tuzar, Z.; Kratochvil, P. *Adv. Colloid Interface Sci.* **1976**, *6*, 201–232.
(3) Zhou, Z.; Chu, B. *Macromolecules* **1987**, *20*, 3089–3091.
(4) Zhou, Z.; Chu, B. *J. Colloid Interface Sci.* **1988**, *126*, 171–180.

(5) Wanka, G.; Hoffmann, H.; Ulbricht, W. *Colloid Polym. Sci.* **1990**, *268*, 101–117.
(6) Brown, W.; Schillén, K.; Almgren, M.; Hvidt, S.; Bahadur, P. *J. Phys. Chem.* **1991**, *95*, 1850–1858.
(7) Brown, W.; Schillén, K.; Hvidt, S. *J. Phys. Chem.* **1992**, *96*, 6038–6044.
(8) Mortensen, K.; Brown, W.; Nordén, B. *Phys. Rev. Lett.* **1992**, *68*, 2340–2343.
(9) Mortensen, K. *Europhys. Lett.* **1992**, *19*, 599–604.
(10) Mortensen, K.; Pedersen, J. S. *Macromolecules* **1993**, *26*, 805–812.
(11) Reddy, N. K.; Fordham, P. J.; Attwood, D.; Booth, C. *J. Chem. Soc., Faraday Trans.* **1990**, *86*, (9), 1569–1572.
(12) Zipper, P. *Acta Phys. Aust.* **1969**, *30*, 143–151.
(13) Glatter, O. *J. Appl. Crystallogr.* **1977**, *10*, 415–421.
(14) *Small Angle X-ray Scattering*; Glatter, O., Kratky, O., Eds.; Academic Press: London, 1982.
(15) Glatter, O.; Gruber, K. *J. Appl. Crystallogr.* **1993**, *26*, 512–518.
(16) Glatter, O. *J. Appl. Crystallogr.* **1979**, *12*, 166–175.
(17) Glatter, O. *Progr. Colloid Polym. Sci.* **1991**, *84*, 46–54.
(18) Glatter, O. *J. Appl. Crystallogr.* **1981**, *14*, 101–108.
(19) Glatter, O.; Hainisch, B. *J. Appl. Crystallogr.* **1984**, *17*, 435–441.
(20) Glatter, O. *J. Appl. Crystallogr.* **1988**, *21*, 886–890.
(21) *Der Ultraschall*; Bergmann, L., Ed.; Hirzel: Stuttgart, 1954.
(22) Glatter, O.; Scherf, G.; Schillén, K. Manuscript in preparation.
(23) Rassing, J.; Attwood, D. *Int. J. Pharm.* **1983**, *13*, 47–55.
(24) Stabinger, H.; Leopold, H.; Kratky, O. *Monatsh. Chem.* **1967**, *98*, 436–438.
(25) Kratky, O.; Leopold, H.; Stabinger, H. *Z. Angew. Phys.* **1969**, *27*, 273–277.
(26) Halperin, A. *Macromolecules* **1987**, *20*, 2943–2946.
(27) Hvidt, S. Unpublished results.
(28) Mortensen, K.; Brown, W. *Macromolecules* **1993**, *26*, 4128–4135.
(29) Schillén, K.; Brown, W.; Johnsen, R. M. *Macromolecules* **1994**, *27*, 4825–4832.
(30) Durchschlag, H.; Zipper, P. *Prog. Colloid Polym. Sci.* **1994**, *94*, 20–39.